LAWRENCE
LIVERMORE
NATIONAL
LABORATORY

Simulations Of Electron Transport For Fast Ignition Using LSP

R. P. J. Town, C. Chen, L. A. Cottrill, M. H. Key, W. L. Kruer, A. B. Langdon, B. F. Lasinski, R. A. Snavely, C. H. Still, M. Tabak, S. C. Wilks, D. R. Welch

May 28, 2004

Disclaimer

SIMULATIONS OF ELECTRON TRANSPORT FOR FAST IGNITION USING LSP

R. P. J. Town[*], C. Chen, L. A. Cottrill, M. H. Key, W. L. Kruer, A. B. Langdon,

B. F. Lasinski, R. A. Snavely, C. H. Still, M. Tabak, and S. C. Wilks

LLNL, 7000 East Ave, Livermore, CA, 94550-9234

D. R. Welch

Mission Research Corp., 5001 Indian School Rd NE, Albuquerque, NM 87110-3946

A crucial issue for the viability of the fast ignition approach to inertial fusion energy is the transport of the ignition pulse energy from the critical surface to the high-density compressed fuel. Experiments have characterized this transport through the interaction of short pulse, high intensity lasers with solid-density targets containing thin K_α fluorescence layers. These experiments show a reasonably well-collimated beam, although with a significantly larger radius than the incident laser beam. We report on LSP calculations of these experiments, which show reasonable agreement with the experimental observations.

1. Introduction

In fast ignition[1] a short-pulse high intensity laser is incident on a pre-compressed DT-fuel assembly. The laser light is deposited at the critical density (which is 1.1×10^{21} cm^{-3} for 1-µm laser light) generating relativistic electrons. These electrons propagate to the high-density (10^{26} cm^{-3}) compressed fuel depositing their energy and igniting the fuel. Fast ignition offers a number of benefits compared to conventional "hot-spot" ignition (where the compression driver is carefully tailored to compress the fuel, but also has to form the ignition region). However, there are a number of technical and scientific uncertainties that must be addressed. The chief uncertainty (and major driver on the short-pulse igniter laser specification) is the coupling efficiency of the incident short-pulse laser to the fuel. There have been many active experimental campaigns to study electron generation and transport through surrogate solid planar targets[2,3]. In this paper we will present hybrid-PIC calculations using the LSP code[4] of these transport experiments.

This paper is structured as follows: The experimental data is summarized briefly in section 2; The LSP code and the choice of the initial electron distribution function is described in section 3; Results from LSP calculations are presented in section 4; and conclusions are drawn in section 5.

2. Review of the experimental data

The two principal diagnostics that have been used to examine electron transport in short-pulse laser-matter interactions are both time integrated imaging diagnostics. The first technique looks at the XUV emission on the rear surface of the target. These XUV images are dominated by near-Planckian thermal emission, which for the measured 68eV

photon energy should make the measurement sensitive to temperatures in the 10 to 100eV range. Shown in figure 1 is a typical XUV image of the rear surface of a 100μm thick Al foil irradiated by the 100-J, 1-ps Vulcan laser at the Rutherford Appleton Laboratory (RAL), UK recently obtained by Key and co-workers[5]. Work is ongoing to convert this into a temperature map. First the XUV images must be converted into absolute brightness. In order to relate the integrated absolute brightness to the temperature a series of Lasnex calculations of isochorically heated Al targets need to be performed. Preliminary analysis suggests that the central 70-μm (fwhm) spot reaches a temperature of approximately 30 eV.

The second technique images Cu K_{α} emission from buried layers of Cu in Al (or CH) targets. The emission size as a function of depth can be obtained by varying the position of the buried fluor layer in the target. K_{α} emission is a two-step process: first an incident electron ejects a K-shell electron and then an outer shell electron fills the vacancy and emits a K_{α} photon. Thus this diagnostics tells us the spatial extent of the hot electron beam. Figure 2 shows a compendium of data for K_{α} emission width as a function of target depth taken from Stephens et al.[6]. These data show a minimum spot diameter of about 70 μm for a bare 25-μm thick Cu foil target. The diameter increases in a 20° half-angle cone with increasing thickness of the Al transport layer in front of the Cu fluor.

3. Defining the initial electron distribution function

In order to model the experiments described above we have used the LSP code originally developed by Mission Research Corporation for use in the ion beam fusion community. LSP is a fully three dimensional hybrid-PIC code capable of running in Cartesian or cylindrical geometries. It employs a direct implicit particle push (based on

the algorithm developed by Friedman, Langdon and Cohen[7]). This algorithm enables larger time steps than conventional explicit PIC codes, which must operate on space and time scales given by the Debye length and plasma frequency, allowing solid density, colder plasmas to be modeled. Such plasmas are more collisional and so LSP incorporates inter- and intra-species collisions based on Spitzer collision frequencies. Finally electrons can be represented as kinetic, or fluid particles. Exchange between the two different types of electrons is user settable and is not based on any physical mechanisms (such as electron runaway). In the fluid description the electrons carry a temperature, which is advanced by a separate energy equation that greatly reduces the effect of numerical cooling. The net effect of these algorithms is to enable LSP to model larger, more dense plasmas for longer simulation times than explicit PIC codes.

However, in order to model the spatial and temporal parameters of the experiment it is not presently possible, in the same simulation, to model the details of the laser-plasma interaction, which generate the hot electron beam. Also, the current version of LSP does not have the correct boundary conditions for electromagnetic waves. Instead we have applied scaling laws derived from small-scale explicit PIC simulations and experimental data to establish the hot electron parameters from the incident laser intensity. The short-pulse Vulcan laser intensity pattern consists of a 10-μm (fwhm) central spot (with a peak intensity of 4.0×10^{19} W/cm^2) that contains approximately 30% of the energy and a much lower intensity ($< 10^{17}$ W/cm^2) broad "halo". Thus the Vulcan laser, like other petawatt lasers around the world, can be approximated by the overlap of a narrow high intensity Gaussian and a low intensity broader Gaussian. To convert this laser intensity pattern into an electron distribution we perform the following steps. First,

the amount of energy that the hot electrons have to carry away from the laser spot is calculated from the conversion efficiency from laser energy to electron energy using the local intensity and a fit to a compilation of experimental data on conversion efficiencies to electron energy at different intensities. These experimental data show a constant conversion efficiency of 10% below 10^{15}W/cm^2; above that threshold intensity and up to 10^{21} W/cm^2 the conversion efficiency, η, depends on the laser intensity, I, according to:

$$\eta = 0.000175 \times I(W/cm^2)^{0.2661}.$$

Next the average energy of the hot electrons is calculated from the scaling law experimentally determined by Beg[8] relating the hot electron temperature, T_{hot}, to the irradiance of the laser $(I\lambda^2)$ according to:

$$T_{hot}(MeV) = 0.1(I\lambda^2/10^{17}W/cm^2\mu m^2)^{1/3}.$$

The beam current density profile can now simply be determined from the ratio of the total electron energy carried at a particular radius and the energy carried by one electron at that radius. Finally a constant-in-space thermal spread is added to the electron energy distribution. The magnitude of the thermal spread is one of the variables that will be adjusted in the next section to compare with the experimental data. We have also performed simulations using the pondermotive scaling law, $T_{hot}(MeV) = (I\lambda^2/10^{19}W/cm^2\mu m^2)^{1/2}$, which predicts a smaller number of electrons with higher energy in the central laser spot compared to the Beg scaling.

4. Simulation results

We have performed simulations of the 100 J, 1 ps Vulcan laser experiments reported by Key[5] and Stephens[6]. Using the procedure outlined in the previous section the calculated total absorbed energy was about 27J. The forward directed electron energy distribution

peaked at about 2MeV in the center of the laser spot and rapidly dropped to a few hundred keV in the wings of the spot (from about 10 to 100 μm). The addition of a constant thermal spread leads to the electrons in the central laser spot to have less angular divergence than the electrons in the wings of the focal spot. The electrons were injected through the left hand boundary into a solid density 100-μm Al^{3+} plasma at 5eV. The perfect conducting boundaries were located at least 50 μm from the plasma on all sides apart from the injection boundary (where the plasma touched the boundary to prevent the target from charging up). All the simulations were two-dimensional using cylindrical (R-Z) geometry.

For comparison with the K_α data a buried 20-μm Cu^{2+} object was inserted into the Al plasma to model the fluor layer. This object recorded the birth-positions of the K_α photons (using cross sections calculated from ITS[9]) which could be transported using ITS to the detector. In the LSP code objects are perfect conductors consequently there was a large resistivity change across the interface between the Al plasma and the Cu object. As the hot electrons transited across this interface we observed a rapid growth in the azimuthal magnetic field to 10MG in agreement with the analytic theory of Bell[10]. However, when a Cu plasma was used instead of the Cu object, the resistivity jump across the interface was much smaller and so no large magnetic field growth was observed at the interface. This suggested that an accurate resistivity model is important to correctly model transport across interfaces and in the plasma. LSP uses Spitzer conductivity, which is only valid for high temperatures (> 100eV for Al). We approximated the resistivity for Al by a simple function in which the resistivity is held fixed at the 100eV Spitzer value below 100eV and obeys Spitzer above 100eV. Figure 3

shows contour plots of the injected electron beam density at 1.6 ps for a calculation using a) Spitzer conductivity and b) the "constant" conductivity model. There is a distinct difference in the shape of the beam propagation between the two calculations. In the Spitzer case the hot electron beam has formed into small filaments whereas the beam shows a more diffuse structure in the "constant" conductivity model calculation. This difference is a direct consequence of the low temperature conductivity model. In the Spitzer model when the first injected electrons cross the plasma they heat the background plasma in channels, increasing the conductivity in the channels, which encourages further injected electrons to propagate along these high conductivity paths. In the constant conductivity case no such high conductivity channels are formed and so the injected electrons do not form into such filamented structures. All subsequent simulations reported here use the constant conductivity model.

The K_α imaging diagnostic gives time-integrated images of the emission generated by the hot electron beam. The diagnostic will record both K_α photons generated by the forward going hot electron beam and by backward going electrons that have been reflected, or "refluxed" at the rear surface. In fact, the trajectories of the hot electrons can be quite complex and show multiple reflections at both the front and back surfaces of the target. Figure 4 shows an example of the hot electron trajectories for particles initially injected at a radius of 10 μm at around the peak of the laser pulse overlaid on a contour plot of the electric field in the z-direction. At early times the hot electrons traverse the target and exit the rear surface of the target. This creates a very large (10^9 V/cm) rear surface electric field that is responsible for accelerating protons to high energies[11] and causes subsequent hot electrons to be reflected or, in conjunction with the large rear-surface magnetic field,

to run along the rear surface of the target. We analyzed the K_α photon generation as a function of time in our LSP calculations. The overall structure of the birth-position of the photons as a function of radius remained relatively constant as a function of time suggesting that the time integrated diagnostic is a good measure of the forward going transport of the hot electron beam. This has been experimentally confirmed by using targets with thicker rear layers of Al (points marked with an "X" in figure 2) that show similar emission radii as the standard 100 μm Al targets.

In order to determine the sensitivity of the emission region to the scaling laws mentioned in section 3 we performed a number of calculations using different amounts of thermal spread. We found very little difference in the K_α emission spot size between the Beg and pondermotive scaling laws when the Cu object was buried 30 μm into the Al plasma. There was greater sensitivity to the initial thermal spread; for example, the emission diameter increased by about 25% when the thermal spread was increased from 200 to 300keV and increased a further 20% when the thermal spread was increased to 600keV. We found reasonable agreement with the experimental data using an injected hot electron spectrum based on the Beg scaling with a thermal spread of 300keV.

Finally we compared the rear surface temperature profile with the XUV imaging diagnostic. The XUV diagnostic is sensitive to the peak temperature so the LSP calculation was advanced for 6 ps until the temporal temperature peak in all of the rear-surface cells had been reached. This peak was recorded for each cell and corrected for real equation of state effects (LSP uses an ideal gas equation of state which over predicts the temperature by about a factor of 3). The LSP calculation predicts a peak temperature of 35eV in an approximate 70-μm spot surrounded by a cooler 10eV pediment. The LSP

calculation shows good agreement with the width of the central XUV image when the injected electrons used Beg scaling and a thermal spread of 300keV. Work continues to establish the experimental temperature.

5. Conclusions

In this paper we have presented results of LSP calculations of recent electron transport experiments. We have shown that the electron transport was sensitive to the conductivity model used. In particular the filamentation of the electron beam was reduced when a more realistic "constant" conductivity was employed. We also showed reasonable agreement between LSP calculations and both the K_α and XUV imaging diagnostics. However, the initial injected electron energy and density distribution was based on simple scaling laws rather than first principles calculations. To address this issue we plan to couple radiation-hydrodynamics, explicit PIC, and LSP calculations together. The hydro-code will be used to predict the amount of pre-formed plasma that is created when the laser pre-pulse interacts with the solid target. The explicit PIC calculations (which resolves the plasma frequency and small spatial scales) will then model the interaction of the laser intensity pattern with the pre-formed plasma to obtain the hot electron distribution. This distribution will then be transported by LSP in a manner similar to reported here. By coupling these three computational techniques together we will be able resolve and simulate in a reasonable time the essential physics necessary to determine the coupling of the short-pulse laser to the compressed fuel.
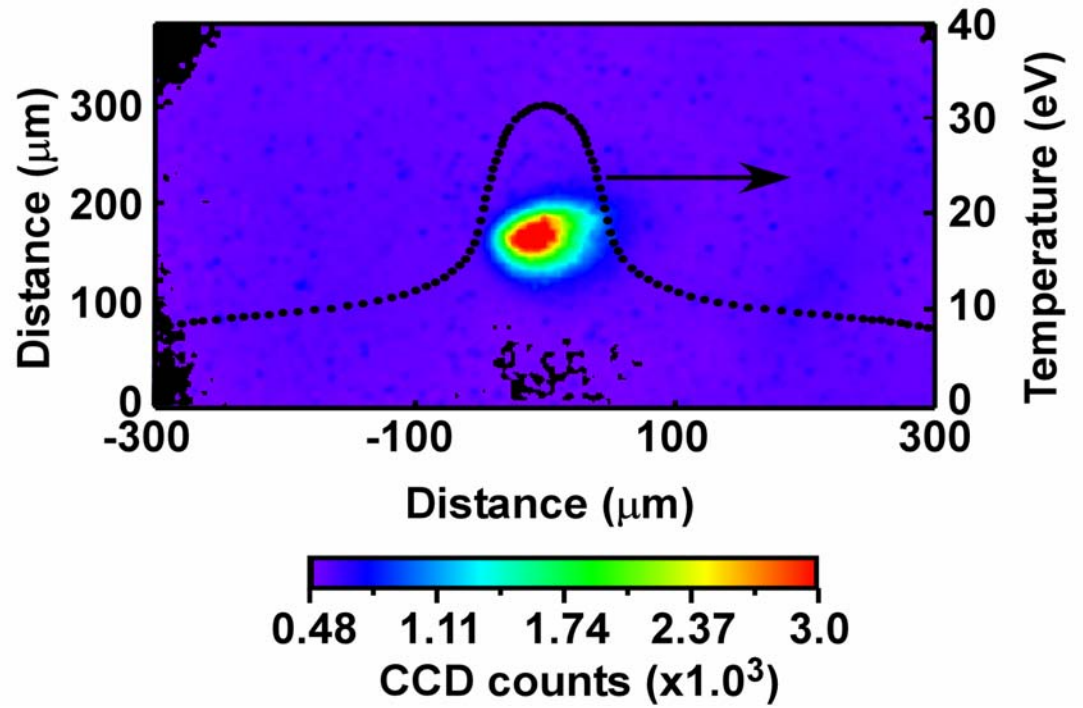
Acknowledgments

Figures

Fig. 1. A contour plot of an XUV image of the rear surface of a 100 μm Al foil illuminated by the short-pulse Vulcan laser, overlaid by the rear-surface temperature profile predicted by the LSP code (dots).
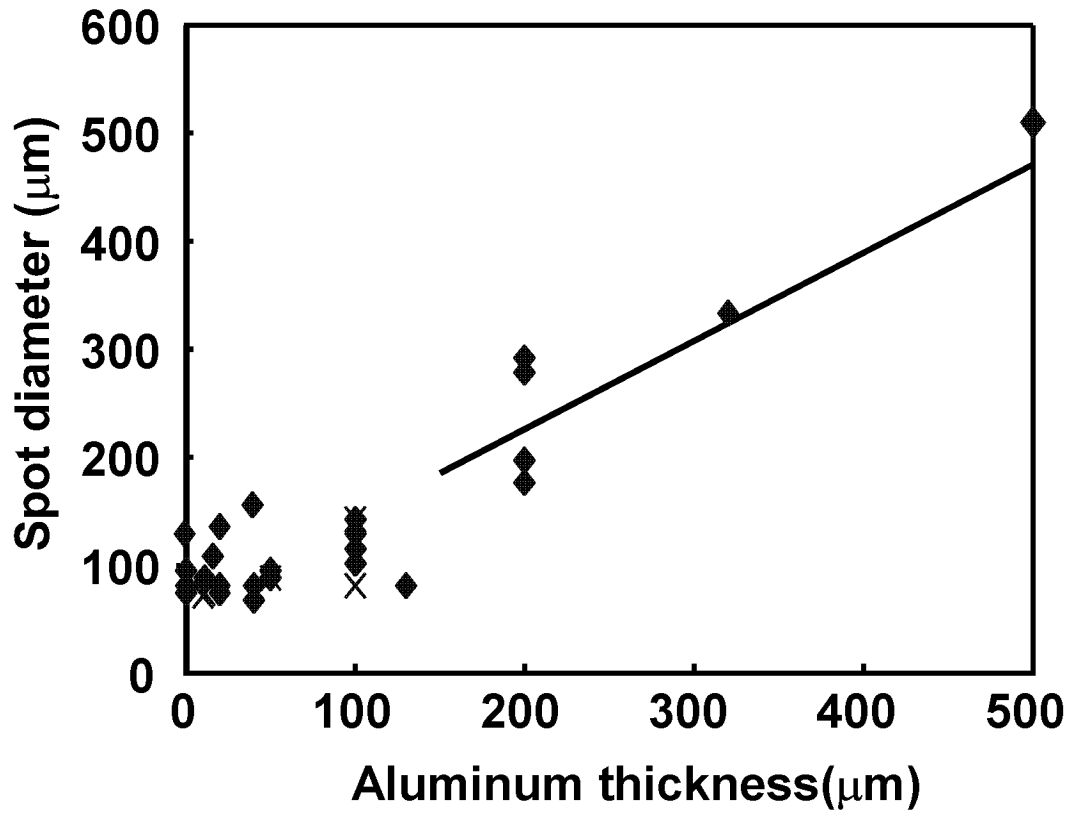
Fig. 2. K$_\alpha$ spot diameter at half-maximum intensity as a function of Al thickness. The line is a linear fit to that data, showing a spreading half-angle of ~20°. The X's indicate targets with thicker back layers to limit refluxing. (Modified from Stephens et al.[6])
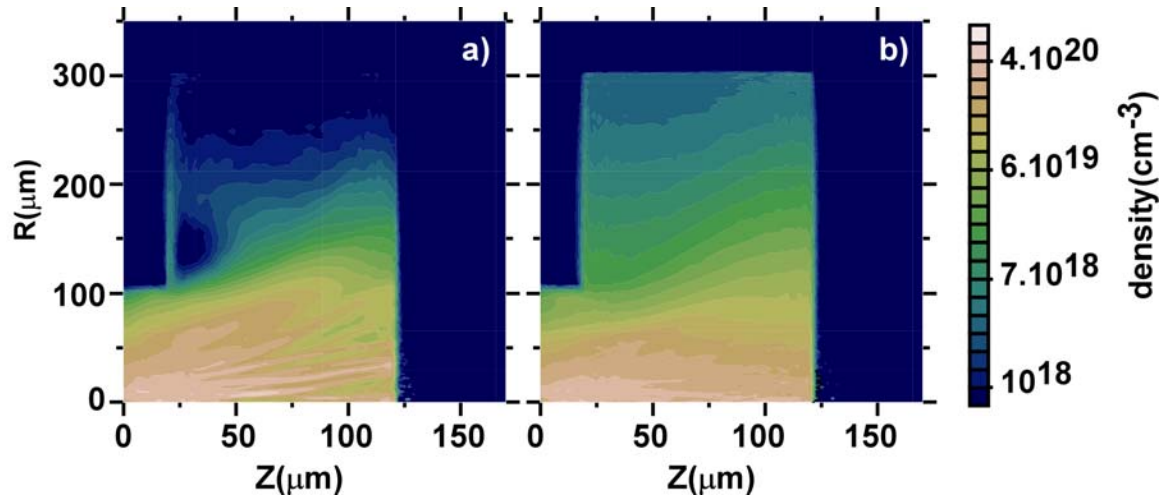
Fig. 3. The injected beam density at 1.6 ps for a calculations using a) Spitzer conductivity and b) the "constant" conductivity model.
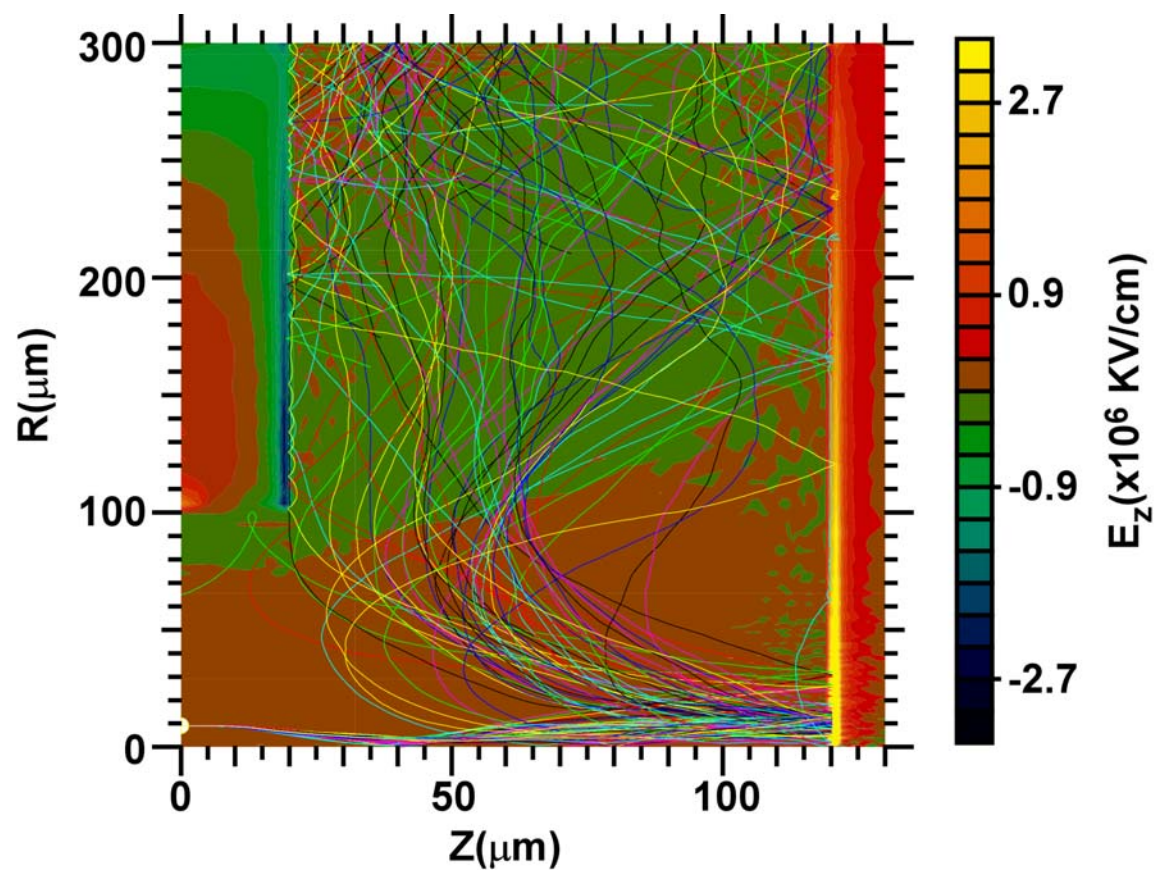
Fig.4. Trajectories of electrons initially injected at a radius of 10μm on top of color contours of the electric field component in the z-direction.

References

[1] M. Tabak, J. Hammer, M. E. Glinsky, W. L. Kruer, S. C. Wilks, J. Woodworth, E. M. Campbell, M. D. Perry, and R. J. Mason, *Phys. Plasmas* **1**, 1626 (1994).

[2] J. A. Koch, M. H. Key, R. R. Freeman, S. P. Hatchett, R. W. Lee, D. Pennington, R. B. Stephens, M. Tabak, *Phys. Rev. E:* **65**, 016410 (2002).

[3] F. Amiranoff, S. D. Baton, L. Gremillet, O. Guilbaud, M. Koenig, E. Martinolli, J. J. Santos, M. R. Le Gloahec, C. Rousseaux, T. Hall, D. Batani, A. Bernardinello, G. Greison, E. Perelli, F. Scianitti, M. H. Key, J. A. Koch, A. J. Mackinnon, R. R. Freeman, R. A. Snavely, C. Andersen, T. E. Cowan, R. B. Stephens, Y. Aglistkiy, *American Institute of Physics Conference Proceedings,* **634**, 28 (2002).

[4] D. R. Welch, D. V. Rose, B. V. Oliver, and R. E. Clark, Nucl. *Inst. Meth. Phys. Res*. A **464**, 134 (2001).

[5] M. H. Key, F. Amiranoff, C. Andersen, S. D. Batani, S.D. Baton, T. Cowan, N. Fisch, R. R. Freeman, L.Gremillet, T. Hall, S. P. Hatchett, J. M. Hill, J. A. King, R Kodama, J. A. Koch, M. Koenig, B. Lasinski, B. Langdon, A. J. MacKinnon, E. Martinolli, P. Norreys, P. Parks,   E. Perelli-Cippo, M. Rabec Le Gloahec, M. Rosenbluth, C. Rousseaux, J. J. Santos, F. Scianitti, R. Snavely, M. Tabak, K Tanaka, R. P. J. Town , T.

Tsutumi, and R. B. Stephens, in *Inertial Fusion Sciences and Applications 2003*, edited

by K. Tanaka, D. D. Meyerhofer, and J. Meyer-ter-Vehn (Elsevier, Paris, 2004).

[6] R. B. Stephens, Y. Aglitskiy, F. Amiranoff, C. Andersen, D. Batani, S. D. Baton, T.

Cowan, R. R. Freeman, T. Hall, S. P. Hatchett, J.M. Hill, M.H. Key, J. A. King, J. A.

Koch, M. Koenig, A. J. MacKinnon, K. L. Lancaster, E. Martinolli, P. Norreys, E.

Perelli-Cippo, M. Rabec Le Gloahec, C. Rousseaux, J. J. Santos, F. Scianitti, R.A.

Snavely, accepted for publication in *Phys. Rev. E:* (2004).

[7] A. Friedman, A. B. Langdon, and B. I. Cohen, *Comments on Plasma Physics & Controlled Fusion* **6***, 225 (1981); D. W. Hewett and A. B. Langdon, *J. Comp. Phys*. **72**, 121 (1987).

[8] F. N. Beg, A. R. Bell, A. E. Dangor, C. N. Danson, A. P. Fews, M. E. Glinsky, B. A.

Hammel, P. Lee, P. A. Norreys, and M. Tatarakis, *Phys. Plasmas* **4**, 447 (1997).

[9] J. A. Halbleib, R. P. Kensek, G. D. Valdez, S. M. Seltzer, and M. J. Berger, *IEEE*

Trans. Nucl. Sci. **NS-39**, 1025 (1992).

[10] A. R. Bell, J. R. Davies and S. M. Guerin, *Phys. Rev. E:* **58**, 2471 (1998).

[11] S. P. Hatchett, C. G. Brown, T. E. Cowan, E. A. Henry, J. S. Johnson, M. H. Key, J. A.

Koch, A. B. Langdon, B. F. Lasinski, R. W. Lee, A. J. Mackinnon, D. M. Pennington, M.

D. Perry, T. W. Phillips, M. Roth, T. C. Sangster, M. S. Singh, R. A. Snavely, M. A.

Stoyer, S. C. Wilks, and K. Yasuike, *Phys. Plasmas* **7**, 2076 (2000)